

Interspatial Attention for Efficient 4D Human Video Generation

RUIZHI SHAO^{*‡}, Tsinghua University, China and Stanford University, United States of America

YINGHAO XU^{*†}, Stanford University, United States of America

YUJUN SHEN, Ant Research, China

CEYUAN YANG, ByteDance Inc., China

YANG ZHENG, Stanford University, United States of America

CHANGAN CHEN, Stanford University, United States of America

YEBIN LIU, Tsinghua University, China

GORDON WETZSTEIN, Stanford University, United States of America

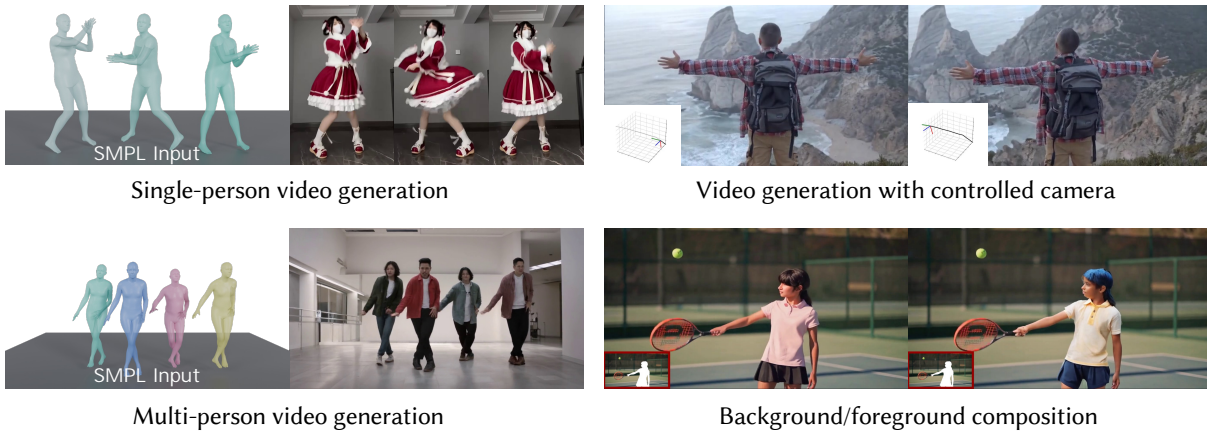


Fig. 1. We introduce interspatial attention as a building block for diffusion transformer–based generative AI models, enabling high-quality video generation of digital humans with a high level of realism, consistency, and identity preservation. Our 4D-aware model enables a wide spectrum of applications, including single-person and multi-person video generation, video generation with controlled camera trajectory, background/foreground composition, among others.

Generating photorealistic videos of digital humans in a controllable manner is crucial for a plethora of applications. Existing approaches either build on methods that employ template-based 3D representations or emerging video generation models but suffer from poor quality or limited consistency and identity preservation when generating individual or multiple digital humans. In this paper, we introduce a new interspatial attention (ISA) mechanism as a scalable building block for modern diffusion transformer (DiT)–based video generation models. ISA is a new type of cross attention that uses relative positional encodings tailored for the generation of human videos. Leveraging a custom-developed video variation autoencoder, we train a latent ISA-based diffusion model on a large corpus of video data. Our model achieves state-of-the-art performance for 4D human video synthesis, demonstrating remarkable motion consistency and identity preservation while providing precise control of the camera and body poses. Our code and model are publicly released at <https://dsaurus.github.io/isa4d/>.

Authors' addresses: Ruizhi Shao^{*‡}, Tsinghua University, Department of Automation, Beijing, China and Stanford University, Department of Electrical Engineering, Stanford, United States of America, jia1saurus@gmail.com; Yinghao Xu^{*†}, Stanford University, Department of Electrical Engineering, Stanford, United States of America, justinyhxu@gmail.com; Yujun Shen, Ant Research, Hangzhou, China, shenyujun0302@gmail.com; Ceyuan Yang, ByteDance Inc., Beijing, China, limbo0066@gmail.com; Yang Zheng, Stanford University, Department of Electrical Engineering, Stanford, United States of America, yzheng18@stanford.edu; Changan Chen, Stanford University, Department of Electrical Engineering, Stanford, United States of America, changanvr@gmail.com; Yebin Liu, Tsinghua University, Department of Automation, Beijing, China, liuyebin@mail.tsinghua.edu.cn; Gordon Wetzstein, Stanford University, Department of Electrical Engineering, Stanford, United States of America, gordon.wetzstein@stanford.edu.

CCS Concepts: • **Computing methodologies** → **Computer vision**.

Additional Key Words and Phrases: human video generation, diffusion model

1 INTRODUCTION

Generating videos of photorealistic humans with full control over camera perspective and body motion is becoming increasingly important for several industries, including visual effects and gaming, teleconferencing, augmented and virtual reality, virtual try-on, robotics, among others.

To unlock these applications, many existing works model, reconstruct, or generate avatars using parametric template–based representations (see Sec. 2.1), including SMPL [Loper et al. 2023]. The realism of template-based avatars, however, is often limited as it is challenging for these approaches to model hair and garments, or accurately simulate deformable parts of the avatar. Emerging human video generation models [Hu et al. 2023a; Shao et al. 2024; Xu et al. 2024; Zhu et al. 2024], on the other hand, have shown great promise for controllable generation of photorealistic digital humans. In contrast to template-based approaches, however, video generation methods lack an understanding of the dynamic 3D nature of avatars, as they do not leverage a 3D model or template. This

^{*}Equal contribution [†] Corresponding author
[‡] Work done during visiting Stanford University

limits multi-frame consistency, identity preservation, the ability to handle multiple characters, and creates other artifacts, for example in the presence of partially occluded body parts.

We identify two core challenges that limit current human video generation models. First, the variational auto-encoders (VAEs) of recent latent video diffusion models (e.g., [Gupta et al. 2023; Luo et al. 2024; Yang et al. 2024b; Yu et al. 2023a; Zhao et al. 2024; Zheng et al. 2024]) do not model the fast movements of human motion well, resulting in blurry and low-quality reconstructions and latent representations that hinder the training process of diffusion models of humans. Second, current video diffusion models lack explicit 3D parametric human modeling. While previous methods project 3D SMPL models onto 2D planes [Shao et al. 2024; Zhu et al. 2024], this leads to insufficient geometric cues, making it difficult to handle complex scenarios like self-occlusions and multi-person interactions.

To address the first challenge, we build a video VAE from the ground up. Our VAE introduces spatial and temporal video compression methods, data augmentation strategies, and regularization terms that, together, provide a memory-efficient and high-quality VAE for latent video diffusion models. Our VAE shows noticeably higher-quality reconstructions than alternative approaches for the fast and subtle dynamics of human motion.

Moreover, we introduce a novel and scalable attention mechanism, Interspatial Attention (ISA), that bridges parametric template representations of humans and emerging video diffusion models. Specifically, ISA implicitly builds correspondences between video frames through learnable 3D–2D relative positional encodings in a cross-attention mechanism tailored to digital humans. The key innovation of ISA lies in its symmetric design: the attention module uses tokens extracted from a 3D template used for conditioning the motion as queries, and tokens extracted from 2D video frames as keys/values. This approach effectively propagates 3D features to 2D space for implicit rendering, while the reverse operation propagates 2D features to 3D space, analogous to 3D reconstruction. Our unique bi-directional attention design creates an implicit rendering–reconstruction mechanism within the diffusion transformer. Unlike methods relying on 2D human representations [Hu et al. 2023b; Shao et al. 2024; Zhu et al. 2024], for example via conditioning, ISA enables seamless integration of 3D template representations within the attention module, thereby handling challenging scenarios such as occlusions and multi-person generation. Furthermore, ISA inherits other advantages of the attention mechanism making it seamlessly compatible with state-of-the-art large-scale diffusion transformer architectures.

We design a video diffusion transformer using the proposed ISA blocks and train it on a large corpus of video data for the purpose of 4D human generation with precise control over human motion, camera movement, and background composition. Our method achieves state-of-the-art performance in 4D human video synthesis, generating long videos with consistent motion and appearance across arbitrary viewpoints. Our specific contributions are:

- We propose a new video VAE design, which facilitates the spatio-temporal compression of videos with fast human motion and builds a well-distributed latent space for diffusion model training.
- We introduce a novel interspatial attention (ISA) block that facilitates the learning of 3D–2D correspondences for 3D condition injection; ISA can be seamlessly integrated into scalable diffusion transformer architectures for 4D human video generation.
- We train a video diffusion model using the proposed VAE and ISA mechanisms. Our system achieves state-of-the-art performance in 4D human video synthesis, enabling flexible camera control, multi-character animation, and background composition.

2 RELATED WORK

2.1 Template-based Human Animation

Template-based approaches for 4D human animation leverage 3D parametric human representations such as SMPL [Loper et al. 2023] in conjunction with efficient neural rendering techniques like NeRF [Kolotouros et al. 2023], DMTeT [Huang et al. 2024b], and Gaussian Splatting [Liu et al. 2023] to generate 3D human animations. These methods, inherently utilizing 3D representations, ensure strict multi-view consistency in the generated animations. Among these, text-to-avatar methods like TADA [Liao et al. 2023], HumanGaussian [Liu et al. 2023], and HumanNorm [Huang et al. 2024b] employ text-to-image diffusion models to optimize a controllable 3D human representation, which is then animated through skinning techniques. However, the dynamic details produced by these methods often lack realism, primarily due to limitations in 3D human body representations and the absence of dynamic priors in text-to-image diffusion models. Alternatively, some methodologies focus on creating personalized avatars through extensive dynamic capture of a specific individual, as exemplified by NeuralActor [Liu et al. 2021], HumanNeRF [Weng et al. 2022], Avatarrex [Zheng et al. 2023b], and AnimatableGaussian [Li et al. 2024]. While these approaches excel in modeling a single person, they suffer from limited generalization capabilities. Moreover, even with the incorporation of generative networks, like GANs [Abdal et al. 2024; Bergman et al. 2022], these methods are constrained by explicit 3D representations, resulting in dynamic effects that fall short of true photorealism and naturalism. To achieve generalization capability and dynamic realism, our method strategically combines the 3D structural benefits of SMPL with the expressive power of emerging video diffusion models, enabling the generation of realistic and consistent 4D human videos.

2.2 Video-based Human Animation

Video models present a promising way for 4D human animation by leveraging deep neural networks, particularly CNNs and Transformers, to directly generate multi-view consistent videos [OpenAI 2024]. These models can implicitly learn spatial relationships and temporal dynamics from video datasets, achieving visually consistent video generations [LumaAI 2024; RunwayAI 2025; Valevski et al. 2024]. Early approaches to human animation primarily focused on 2D

image animation based on GANs [Goodfellow et al. 2014]. GAN-based approaches [Siarohin et al. 2019a,b, 2018; Tian et al. 2021; Wang et al. 2021, 2020] leverage the generative capabilities of adversarial networks [Goodfellow et al. 2014; Mirza and Osindero 2014] to animate human by transforming reference images according to input motion. These methods typically employ warping functions to generate sequential video frames, aiming to fill in missing regions and enhance visually implausible areas within the generated content. While showing promise in dynamic human generation, GAN-based methods often struggle with generalizable motion transfer, particularly when there are significant variations in human identity and scene dynamics between the reference image and the source video, leading to unrealistic visual artifacts and temporal inconsistencies in the synthesized videos.

Diffusion models, known for their superior generation quality and stable controllability, have been successfully applied to human image animation [Bhunia et al. 2023; Hu et al. 2023a; Karras et al. 2023; Shao et al. 2024; Wang et al. 2023; Xu et al. 2024; Zhu et al. 2024]. These models employ various strategies, such as reference cross-attention blocks and optical flow in latent space, to enhance the visual fidelity and consistency of generated videos. For instance, Animate Anyone [Hu et al. 2023a] employs a UNet-based ReferenceNet to inject features from reference images, and incorporates human motion through pose guidance network. While diffusion models achieve realistic and high-quality 2D video generation, these methods struggle to generate multi-view consistent videos with physically correct content. The key challenge in extending these models to 4D video generation lies in effectively incorporating 3D conditions. Recent works have begun exploring the injection of camera conditions [He et al. 2024; Yang et al. 2024a] and 3D SMPL [Shao et al. 2024; Zhu et al. 2024]. Champ [Zhu et al. 2024] employs SMPL as an enhanced animation condition to preserve 3D shape identity and achieve improved human motion control. Human4DiT [Shao et al. 2024] further leverage a diffusion transformer with temporal and view transformers, simultaneously incorporating 3D SMPL and cameras for enhanced 4D human video generation. However, these methods typically require rendering 3D SMPL into 2D maps, such as normal maps, resulting in the loss of 3D structural information during camera projection. This limitation makes it particularly challenging to handle self-occlusion and multi-person video generation scenarios. To address this challenge, we propose interspatial attention, which efficiently builds the explicit correspondences between 3D SMPL and 2D videos.

2.3 Variational Autoencoder

Recent advances in two-stage generative model pipelines have highlighted the crucial role of VAEs [Kingma 2013] in compressing 2D signals into latent space. Early approaches focused on discrete codebook compression, as pioneered by VQ-VAE [Van Den Oord et al. 2017] and enhanced by VQ-GAN [Esser et al. 2021] and ViT-VQGAN [Yu et al. 2021] through adversarial training and transformer architectures, but suffered from limited reconstruction quality due to discrete tokens. Later works such as 3D-VQVAE [Yan et al. 2021] and 3D-VQGAN [Ge et al. 2022; Yu et al. 2023a] extended the discrete compression framework to the video domain. Building upon

this, MAGVITV2 [Yu et al. 2023b] and CViViT [Villegas et al. 2022] further introduced causal 3D convolutions and transformers to enable arbitrary-length video compression, yet the discrete token space remained a fundamental limitation for generation quality. In parallel, continuous latent space methods emerged, with CV-VAE [Zhao et al. 2024] and W.A.L.T. [Gupta et al. 2023] demonstrating impressive results on general video content through 3D VAE architectures and causal temporal modeling. Recently, large-scale video models, including CogVideoX [Yang et al. 2024b], Mochi [Mochi-Team 2024], and Cosmos [Reda et al. 2024], have extended this approach by developing their VideoVAEs for video compression. However, these methods struggle with human videos due to their deformable and articulated nature, where fast local and global motions lead to poor reconstruction quality and suboptimal latent distributions. Our work addresses these limitations through advanced data augmentation and latent regularization specifically designed for fast human video compression, facilitating high-quality diffusion model training.

3 OVERVIEW

In the remainder of this paper, we first detail the design and training of our video VAE in Sec. 4. Then, we briefly review basic attention mechanisms in Sec. 5.1, before introducing our new interspatial attention in Sec. 5.2. In Sec. 5.3, we discuss how to incorporate interspatial attention into a modern diffusion transformer architecture for human video generation with control over identity, camera pose, and background.

Our human video generator takes as input animated SMPL poses for each character as well as a reference image, which can be either a photograph or a generated image. We can optionally specify the camera trajectory and the background. The output is a video that adheres to the motions defined by the input SMPL poses and the identity structure of the reference image.

4 VIDEO AUTOENCODER

Latent diffusion models employ variational autoencoders (VAEs) to compress images or videos into compact latent representations that enable computationally efficient generation [Rombach et al. 2022]. However, we find that existing VAEs struggle to capture the rapid and complex dynamics of human motion. To address the limitation, we present a novel VAE that is built from the ground up to effectively encode such complexity in video data.

Our compression model is inspired by MAGVITV2 [Yu et al. 2023b] and W.A.L.T. [Gupta et al. 2023], adopting their unified VAE architecture for joint image–video compression with support for videos of arbitrary length. Formally, let $\mathcal{V} = \{\mathbf{v}_i\}_{i=1}^{1+T}$ denote a video clip consisting of $1 + T$ frames where each frame $\mathbf{v}_i \in \mathbb{R}^{H \times W \times 3}$. The encoder $E(\cdot)$ compresses the video into spatio-temporal latent representations $\mathcal{Z} = \{\mathbf{z}_i\}_{i=1}^{1+t}$, with each latent $\mathbf{z}_i \in \mathbb{R}^{h \times w \times c}$. The corresponding decoder $D(\cdot)$ reconstructs the video frames from the latent representations. To achieve efficient compression, the encoder downsamples spatially by a factor $f_s = H/h = W/w$ and temporally by a factor $f_t = T/t$. By default, we use $f_s = 8$, $f_t = 4$, and set the latent dimension as $c = 16$. In the following, we present the details of the network architecture (Sec. 4.1), training strategy (Sec. 4.2) and the evaluation protocol (Sec. 4.3) for the proposed VideoVAE.

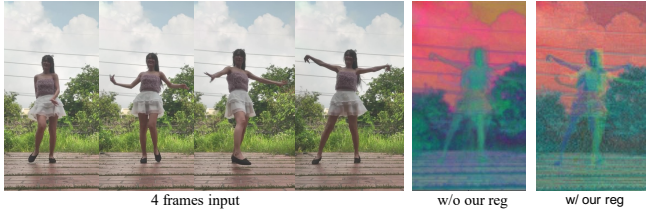


Fig. 2. **Last-frame bias.** The latent tends to compress the final key frame in each temporal window (center right). After adding the *image-decoding regularization*, the latent maintains balanced temporal information distribution across frames (right).

4.1 Architecture

We extend the pretrained image VAE from Stable Diffusion 3 (SD3) [Esser et al. 2024] into a 3D architecture to model temporal dynamics in videos. The original SD3 VAE architecture consists of cascaded residual blocks interleaved with downsampling (average pooling) and upsampling (resizing plus convolution) layers. To enable video compression, we inflate this 2D architecture by extending all convolutions to include a temporal dimension, transforming them into 3D convolutions. For joint image–video compression, we replace regular 3D convolutions with temporally causal 3D convolutions, similar to MAGVITV2 [Yu et al. 2023b] and W.A.L.T. [Gupta et al. 2023]. The causal 3D convolutions ensure that each frame depends only on previous frames, allowing the model to handle both single images and videos of arbitrary length. Following the SD3 VAE, we enhance reconstruction quality using adversarial losses from a discriminator. While typical image compression frameworks only supervise individual frames, we introduce a 3D discriminator by replacing 2D convolutions with 3D convolutions, thereby capturing temporal dynamics in the reconstructed video. Despite these modifications, we observe that the trained video VAE model still struggles with fast, articulated human motions, and the spatio-temporal latents show suboptimal distributions as demonstrated in Fig. 2 that hinder the subsequent diffusion training. We thus propose novel training strategies (Sec. 4.2) to address these limitations.

4.2 Training

Next, we introduce two novel training strategies: spatio-temporal data augmentation and image-decoding regularization, designed to achieve high reconstruction fidelity and well-structured latent representations for complex human videos.

Spatio-temporal Data Augmentation. Human motion in videos is inherently challenging to model due to frequent self-occlusions, complex human body and garment deformations, and motion blur. To tackle these challenges, we introduce two complementary data augmentation strategies as described below:

1) *Random Structured Motion.* To address large spatial displacements (such as squatting and jumping), we randomly translate each video frame in different directions and at varying velocities. This structured motion perturbation encourages the model to learn how to reconstruct significant spatial shifts, enhancing its robustness in handling challenging global motions.

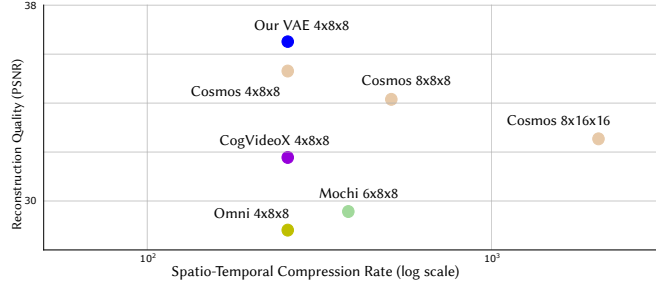


Fig. 3. **Comparison of video tokenizers on spatio-temporal compression rate (log scale) vs. reconstruction quality (PSNR).** Each point represents a trade-off between compression ratio and reconstruction quality for different tokenizer configurations. Our method achieves better reconstruction quality than existing video tokenizers.

Table 1. **Quantitative comparison of video tokenizers.** While omitting regularization terms slightly improves reconstruction quality, adding regularization makes video diffusion model training more efficient.

Method	PSNR \uparrow	SSIM \uparrow	LPIPS \downarrow	FVD \downarrow
Mochi	31.78	0.946	0.036	31.94
Cosmos 4 \times 8 \times 8	35.31	0.972	0.028	15.72
CogVideoX	32.54	0.954	0.035	25.85
Ours (w/o reg)	36.71	0.980	0.014	11.57
Ours	36.59	0.981	0.015	12.16

2) *Dynamic Speed Adjustment.* Targeting fast local motions (such as fast hand movements), we modulate video frame rates to generate diverse motion speed samples. This temporal adaptation strategy creates varied temporal densities of motion representation, effectively improving the model’s robustness to fast local movements.

Image-decoding Regularization. The shape of the latent distribution plays a crucial role in the performance of diffusion model training. For example, a dataset whose latent space distribution is irregularly shaped or which has a high variance might be more challenging to be learned by a diffusion model. While following prior works [Esser et al. 2024; Rombach et al. 2022] to impose a slight KL-penalty to notch the latent distribution towards a normal distribution, we observe a “last-frame bias” phenomenon in the learned latents of our video VAE—the latent tends to primarily compress the last frame in each temporal window, as shown in Fig. 2. This last-frame-biased compression makes the latent distribution suboptimal for diffusion model training, causing severe artifacts during frame transitions at temporal window boundaries in generated videos, especially in videos with fast motion.

To address this problem, we introduce an image-decoding regularization term that incorporates an auxiliary image decoder to reconstruct input video frames. Specifically, we decompose each 16-channel latent z_i into four 4-channel sub-latents, each independently decoding individual frames by the auxiliary image decoder. This frame-wise independent decoding serves as an implicit constraint



Fig. 4. **Qualitative comparison of video VAEs.** We compare the reconstruction quality of different VAEs using a crop of a 1920×1080 video for our VAE, Mochi, CogVideoX, and Cosmos. Mochi’s VAE is noticeably worse than all others with Cosmos also being blurrier than CogVideoX and ours.

for balanced temporal information distribution, mitigating the last-frame bias and producing well-structured latents that benefit diffusion training.

Data and Objectives. We utilize the action recognition dataset Kinetics-600 [Kay et al. 2017] and the human video generation dataset Human4DiT [Shao et al. 2024], comprising 600K videos for VAE training. To enable inference on long videos, we propose a two-stage training scheme: first training our model on short (33 frames) sequences, then fine-tuning it on long (97 frames) sequences. We train our video VAE using multiple objectives: the L_1 loss \mathcal{L}_{L1} , perceptual loss \mathcal{L}_p , KL divergence loss \mathcal{L}_{KL} , 2D GAN loss \mathcal{L}_{2DGAN} , 3D GAN loss \mathcal{L}_{3DGAN} , and a regularization term for the image decoder \mathcal{L}_{reg} :

$$\mathcal{L} = \lambda_{L1}\mathcal{L}_{L1} + \lambda_p\mathcal{L}_p + \lambda_{KL}\mathcal{L}_{KL} + \lambda_{reg}\mathcal{L}_{reg} \quad (1)$$

$$+ \lambda_{3DGAN}\mathcal{L}_{3DGAN} + \lambda_{2DGAN}\mathcal{L}_{2DGAN}, \quad (2)$$

where λ_{L1} , λ_p , λ_{KL} , λ_{reg} , λ_{2DGAN} and λ_{3DGAN} are the weights for each respective loss term.

4.3 Evaluation

Data and Metrics. To evaluate the video VAE, we curate an evaluation dataset of 200 high-resolution human videos featuring multi-person interactions, complex textures, and fast motions. We evaluate reconstructed video quality using peak signal-to-noise ratio (PSNR). For comparison, we select state-of-the-art video VAE baselines including the Cosmos tokenizer [Reda et al. 2024] and video VAE models from Mochi [Mochi-Team 2024], and CogVideoX [Yang et al. 2024b].

Analysis. As shown in Fig. 3, our video VAE substantially outperforms the Cosmos and Mochi tokenizers. Fig. 4 and Tab. 1 present qualitative and quantitative comparisons on videos featuring fast

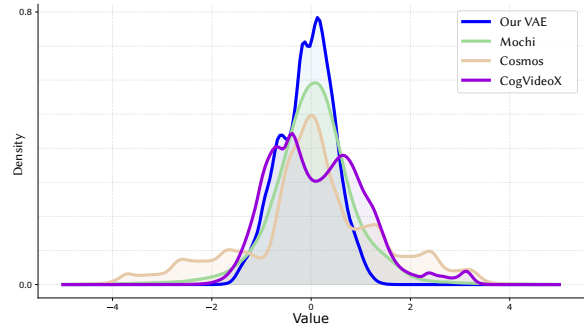


Fig. 5. **Comparison of latent distribution from different approaches.** We visualize the latent distributions on the evaluation videos. Our method yields well-structured latent representations compared to baseline methods.

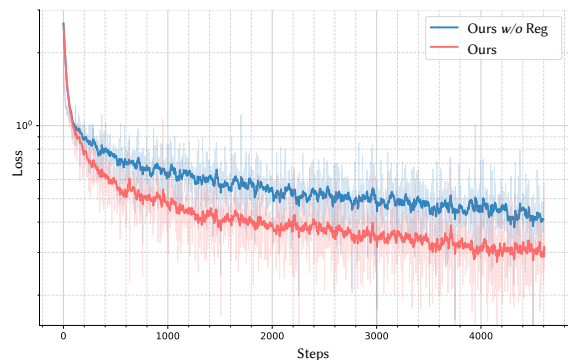


Fig. 6. **Ablation study of latent regularization.** We compare training loss curves of diffusion transformers using latents from VAEs trained with and without regularization.

human motion and self-occlusion. Our model more effectively preserves structural and high-frequency details while introducing less visual distortion compared to the baselines. To comprehensively evaluate the suitability of the latent space for generation, we visualize the latent distributions on the evaluation datasets in Fig. 5. Our model produces a structured latent distribution that more closely approximates a Gaussian distribution than some other latent spaces, indicating that our latent space might be easier to be learned by a diffusion model than others.

Additional qualitative examples are included in the supplement.

Ablation on VAE regularization. To evaluate our regularization term, we train diffusion transformers using latents from two of our VAE variants – with and without regularization. As shown in Fig. 6, the training loss reveals that regularized VAE produces more structured latent distributions that facilitate better and faster diffusion model training.

5 ATTENTION FOR 4D HUMAN VIDEO GENERATION

Attention [Vaswani et al. 2017] is widely recognized as a fundamental mechanism for capturing spatial relationships in sequences

or images. However, standard attention operations require comparing pairwise correlations in the data, making them inefficient when transitioning from 2D images to 3D or 4D generation tasks. In this section, we first review the basics of self-attention and cross-attention mechanisms. We then introduce a novel *interspatial* attention formulation that uses correspondences between image frames and parametric template meshes, thereby enabling efficient 4D human video generation.

5.1 Basic Attention Mechanisms

Self-Attention. Attention enables networks to learn feature relationships through weighted importance scores. The basic self-attention operation is formulated as:

$$Q = XW_q, \quad K = XW_k, \quad V = XW_v, \quad (3)$$

$$\text{ATTENTION}(Q, K, V) = \text{softmax}\left(\frac{QK^T}{\sqrt{d}}\right)V, \quad (4)$$

where Q , K and V denotes query, key, and value matrices, respectively. $W_q \in \mathbb{R}^{d \times d_x}$, $W_k \in \mathbb{R}^{d \times d_x}$ and $W_v \in \mathbb{R}^{d \times d_x}$ are the learned projection matrix of input feature X , where d is the learned feature dimension and d_x is the input feature dimension.

Cross-Attention. The attention mechanism can be extended to relate different feature spaces, thereby modeling inter-modality relationships. In this case, Q comes from one domain while K , V come from another. A common example is to relate text features Y and image features X in text-conditioned diffusion models [Rombach et al. 2022] as:

$$Q_x = XW_q, \quad K_y = YW_k, \quad V_y = YW_v, \quad (5)$$

$$\text{CROSSATTENTION}(X, Y) = \text{softmax}\left(\frac{Q_x K_y^T}{\sqrt{d}}\right)V_y. \quad (6)$$

Although text-to-image generation is a popular application, cross-attention generalizes to other modalities beyond text and images.

Transformer Block Integration. Attention modules are frequently combined with Layer Normalization (LayerNorm) and a Feed-Forward Network (FFN) to form transformer blocks, which serve as a fundamental component in many diffusion models. Specifically, a transformer block $Y = \text{TRANSFORMER}(X)$ comprises:

$$\begin{aligned} X &= X + \text{ATTENTION}(\text{LayerNorm}(X)), \\ Y &= X + \text{FFN}(\text{LayerNorm}(X)), \end{aligned} \quad (7)$$

where X represents the input features, and the attention operation could be either self-attention within the same modality or cross-attention between different modalities as described above.

5.2 Interspatial Attention

Basic attention mechanisms learn correlations between different parts of an image or video by considering all other parts as equally viable candidates, thus providing flexibility but suffering from inefficiency for 3D or 4D generation tasks. In the context of 4D human video generation, the question arises: how can we effectively identify and attend to corresponding features across video frames without resorting to exhaustive comparisons between all features? Our interspatial attention (ISA) mechanism builds on an intuitive insight:

when generating 4D human videos conditioned on SMPL poses, the SMPL template provides rough correspondences across frames. We leverage these correspondences to design an attention mechanism for 4D human video generation, which informs the network where to look for relevant correspondences.

ISA implements this intuition in an efficient manner. Inspired by cross attention, ISA is an attention mechanism tailored for 4D human video generation that includes a carefully designed relative interspatial position encoding to provide the correct 4D geometric cues, enabling networks to capture the inherent 3D–2D relationships, as illustrated in Fig. 7.

Interspatial Attention without Positional Encoding. To incorporate correspondences between the same parts of a digital human in different frames, we leverage the deformable 3D SMPL representation in combination with a cross-attention mechanism. This enables direct interaction between 3D human pose and 2D video features.

Specifically, we first sample a set of points on the surface of a SMPL mesh and construct a point sequence in global coordinate frame $\mathcal{G} = \{\mathbf{G}_i\}_{i=1}^{1+T}$, which we then convert into 3D tokens $\mathcal{Y} = \{\mathbf{Y}_i\}_{i=1}^{1+T}$ by a shallow MLP encoder $F_{\text{mlp}}(\cdot)$ using the sinusoidal position encoding [Vaswani et al. 2017] $\text{PE}(\cdot)$:

$$\mathbf{Y}_i = F_{\text{mlp}}(\text{PE}(\mathbf{G}_i)). \quad (8)$$

The 2D latents are then transformed from raw videos with our video VAE encoder: $\mathcal{Z} = \{\mathbf{z}_i\}_{i=1}^{1+t} = E(\mathcal{V} = \{\mathbf{v}_i\}_{i=1}^{1+T})$ with a temporal downsample factor of $f_t = T/t$. Because the latents are downsampled along the temporal dimension, we conditioned a single latent \mathbf{z}_j with the corresponding SMPL poses $\mathcal{Y}_j = \{\mathbf{Y}_i\}_{i=1+f_t \times (j-1)}^{1+f_t \times j}$ using cross attention:

$$\mathbf{z}'_j = \text{CROSSATTENTION}(Q(\mathbf{z}_j), K(\mathcal{Y}_j), V(\mathcal{Y}_j)), \quad (9)$$

where $Q(\cdot)$, $K(\cdot)$ and $V(\cdot)$ are flattened learnable linear projection. However, we find this simple cross attention leads to poor training convergence and fails to achieve accurate 3D pose conditioning (see e.g. Fig. 14). The network is required to infer geometric correspondences between the 2D video data and the 3D SMPL poses in the absence of explicit guidance, leading to suboptimal results.

Interspatial Positional Encoding (ISPE). Inspired by implicit coordinate networks [Mescheder et al. 2019; Mildenhall et al. 2020; Park et al. 2019], we introduce ISPE to explicitly guide the network in building 3D–2D relationships. ISPE aims to model the spatial correspondence between 3D SMPL tokens and 2D video tokens by transforming their coordinates into a unified coordinate system using the known camera parameters. Specifically, we project the coordinates of 3D SMPL tokens $\mathbf{g} = (x, y, z, w = 1)$ to normalized device coordinate (NDC) space using the modelview-projection matrix \mathbf{M} :

$$\begin{aligned} \mathbf{g}_{\text{clip}} &= [x_{\text{clip}}, y_{\text{clip}}, z_{\text{clip}}, w_{\text{clip}}]^T = \mathbf{M}\mathbf{g}, \\ \mathbf{g}_{\text{ndc}} &= \begin{bmatrix} x_{\text{clip}} & y_{\text{clip}} & z_{\text{clip}} \\ w_{\text{clip}} & w_{\text{clip}} & w_{\text{clip}} \end{bmatrix}^T. \end{aligned} \quad (10)$$

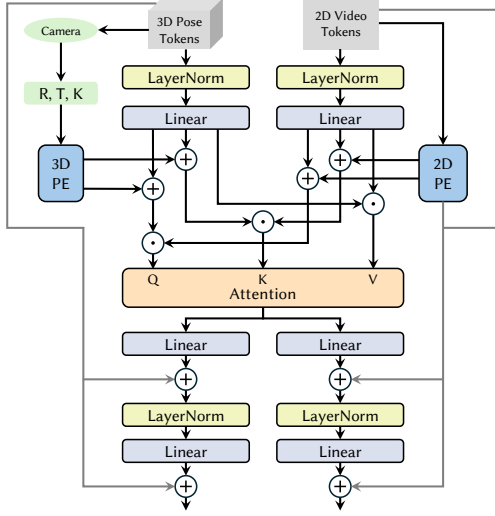


Fig. 7. **Symmetric Interspatial Attention Block.** The attention block is a symmetric operation on 3D SMPL tokens and 2D video tokens. Concatenation is indicated by \odot and element-wise addition by $+$.

For 2D video tokens, we project their coordinates in (latent) pixel space $\mathbf{s} = [s_x, s_y]^T$ onto a 3D plane with zero depth in NDC space:

$$\mathbf{s}_{ndc} = (2s_x/w - 1, 2s_y/h - 1, 0), \quad (11)$$

where s_x and s_y are the image coordinates at the latents, and w, h denote the latent width and height. After obtaining the coordinates in this unified (NDC) space, we apply a sinusoidal positional encoding $\text{PE}(\cdot)$ to compute the ISPE. We then incorporate ISPE into our proposed interspatial attention by adding it to both token:

$$\mathbf{z}'_j = \text{ISATTENTION}(\text{Q}(\mathbf{z}_j + \text{PE}(\mathbf{s}_{ndc})), \text{K}(\mathcal{Y}_j + \text{PE}(\mathbf{g}_{ndc})), \text{V}(\mathcal{Y}_j + \text{PE}(\mathbf{g}_{ndc}))). \quad (12)$$

By encoding features in a unified coordinate system, ISPE provides explicit geometric guidance for the attention mechanism. This spatial awareness helps establish effective 3D–2D correspondences during feature interaction, improving the quality of 3D conditioning.

Symmetric Interspatial Attention (ISA). Unlike previous approaches that only condition the video generation model using 2D projections of the SMPL template from a fixed viewpoint [Hu et al. 2023b; Xu et al. 2024; Zhu et al. 2024], we propose a symmetric interspatial attention mechanism that enables bidirectional information flow between 3D and 2D spaces, inspired by the mm-DiT block in SD3 [Esser et al. 2024]. Specifically, we utilize 3D and 2D token features as queries and values respectively, with the ISPE guiding the attention:

$$\mathcal{Y}'_j = \text{ISATTENTION}(\text{Q}(\mathcal{Y}_j + \text{PE}(\mathbf{g}_{ndc})), \text{K}(\mathbf{z}_j + \text{PE}(\mathbf{s}_{ndc})), \text{V}(\mathbf{z}_j + \text{PE}(\mathbf{s}_{ndc}))), \quad (13)$$

$$\mathbf{z}'_j = \text{ISATTENTION}(\text{Q}(\mathbf{z}_j + \text{PE}(\mathbf{s}_{ndc})), \text{K}(\mathcal{Y}_j + \text{PE}(\mathbf{g}_{ndc})), \text{V}(\mathcal{Y}_j + \text{PE}(\mathbf{g}_{ndc}))), \quad (14)$$

In this way, our approach implicitly performs simultaneous rendering (3D-to-2D) and reconstruction (2D-to-3D) by allowing features to interact in both directions. This improved feature interaction results in more effective conditioning of 3D structural information, facilitating consistent and high-quality 4D human video generation. As shown in Fig. 7, we then integrate the symmetric ISA with LayerNorm [Lei Ba et al. 2016] and a Feedforward Network (FFN) [Vaswani et al. 2017] to form a Symmetric Interspatial Transformer Block, similar to Eq. (7). This block serves as a crucial component in our video diffusion transformer architecture.

5.3 Interspatial Diffusion Transformer (ISA-DiT)

Based on our video VAE and the ISA attention, we now discuss how to integrate it into a diffusion transformer architecture for human video generation that effectively bridges 3D structural information and 2D video features. The core change to a conventional DiT architecture is the addition of parallel symmetric branches: a 3D branch for learning SMPL features and a 2D branch for video features. These branches are interconnected through our ISA block. Our framework, illustrated in Fig. 8, uses a single input image as conditioning information and simultaneously injects the included human identity into both 3D and 2D branches for identity consistency across generated frames. Furthermore, we introduce a switchable background conditioning module, which enables flexible composition between human videos and various background settings. We discuss the unique components of our architecture in the following.

Symmetric Diffusion Branch. Our framework employs a symmetric diffusion architecture comprising specialized transformer modules (Fig. 8). Building upon SD3’s architecture, we extend it for video generation by incorporating temporal transformer blocks between existing 2D image transformer blocks. In this enhanced architecture, 2D video tokens \mathbf{z} are first processed through a spatial transformer block:

$$\mathbf{z}_s = \text{SPATIALTRANSFORMER}(\mathbf{z}), \quad (15)$$

followed by a temporal transformer that establishes frame-wise temporal correlations:

$$\mathbf{z}_{st} = \text{TEMPORALTRANSFORMER}(\mathbf{z}_s). \quad (16)$$

For effective 3D SMPL conditioning, we encode sampled SMPL points into 3D tokens as described in Eq. (8). The 3D SMPL tokens \mathbf{Y} are processed through a temporal transformer block to establish temporal continuity across consecutive SMPL representations:

$$\mathbf{Y}_t = \text{TEMPORALTRANSFORMER}(\mathbf{Y}). \quad (17)$$

These 3D tokens are then processed by the symmetric ISA transformer block, which bridges the gap between 3D SMPL poses and 2D videos, enabling seamless interaction:

$$\mathbf{Y}'_t, \mathbf{z}'_{st} = \text{ISATRANSFORMER}(\mathbf{Y}_t, \mathbf{z}_{st}). \quad (18)$$

Finally, the learned 2D video features interact with the camera pose and reference image through cross-attention blocks, which we describe in detail in the following.

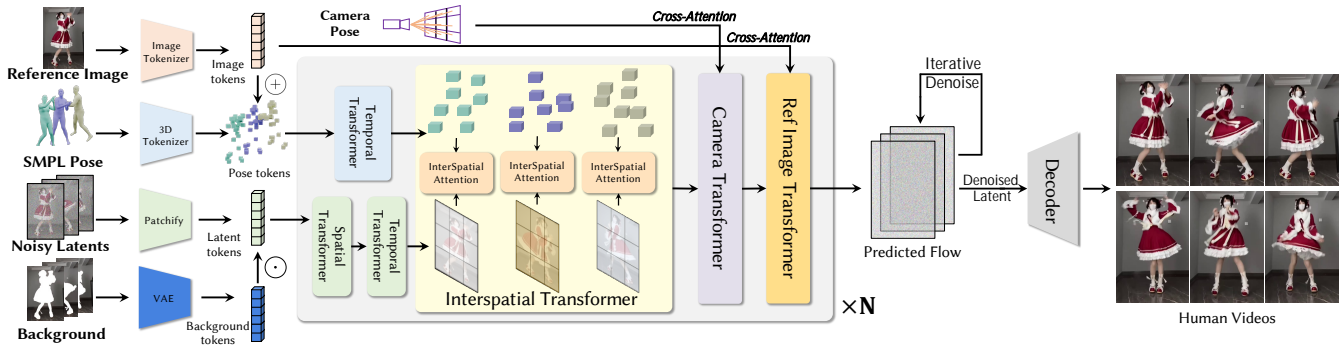


Fig. 8. **ISA-DiT pipeline.** Overview of our diffusion transformer architecture for 4D human generation taking the reference image, SMPL condition, camera poses, and background videos as input. Our framework starts by tokenizing 3D SMPL conditions. In parallel, 2D video tokens (i.e., “noisy latents”) are optionally composited with background elements and processed through a cascade of disentangled spatial and temporal transformer blocks, enabling efficient modeling of spatio-temporal relationships. These tokens then seamlessly interact with pose tokens via our Interspatial Transformer Block, facilitating effective 3D-aware conditioning. The generated features are further enhanced through Plücker camera embeddings for precise view control and interact with reference image features through cross attention to ensure consistent identity preservation. The entire framework is optimized using a flow-based diffusion formulation, enabling high-quality 4D human generation with controllable pose, viewpoint, and identity.

Identity Conditioning Module. To ensure identity consistency across diverse views and temporal frames, we propose a novel identity injection strategy that simultaneously incorporates human identity information into both 3D SMPL and 2D video features. Specifically, our identity condition module has two sub-modules.

For the 3D SMPL branch, we first extract the latent feature \mathbf{z}_{ref} from reference image \mathbf{I}_{ref} with the VideoVAE. We then estimate the SMPL models of the reference image and perform pixel-aligned feature propagation onto 3D SMPL tokens:

$$\mathbf{Y} = \mathbf{Y} + \text{GRIDSAMPLE}(\mathbf{z}_{ref}, \pi_y(\mathbf{Y})), \quad (19)$$

where $\pi_y(\mathbf{Y})$ are the projected 2D reference image coordinates for the 3D SMPL tokens. This 3D propagation enhances the temporal consistency of human identity.

For 2D video features, we inject the reference image through both local concatenation and global cross-attention mechanisms:

$$\mathbf{z}_l = \text{CONCAT}([\mathbf{z}, \mathbf{z}_{ref}]), \quad (20)$$

$$\mathbf{z}_g = \text{CROSSATTENTION}(\mathbf{z}, \text{CLIP}(\mathbf{I}_{ref})), \quad (21)$$

where the concatenation operation preserves fine-grained identity details, and the CLIP embedding in cross-attention ensures global identity consistency.

Camera Conditioning Module. To achieve precise camera view control, we parameterize the camera poses into Plücker coordinates for detailed geometric modeling following prior works [He et al. 2024]. We first encode the rotation and translation of camera parameters into Plücker images \mathbf{c} . Considering the temporal downsampling of our videos, we concatenate multiple camera embeddings corresponding to the same latent frame across channels:

$$\mathbf{c}_{latent} = \text{CONCAT}([\mathbf{c}_1, \dots, \mathbf{c}_k]), \quad (22)$$

and the camera condition is then injected via cross-attention:

$$\mathbf{z}_{cam} = \text{CROSSATTENTION}(\mathbf{z}, \mathbf{c}_{latent}). \quad (23)$$

Background Conditioning Module. Our framework enables flexible background composition through a conditional injection mechanism. The background videos \mathbf{v}_{bg} are first encoded through our videoVAE encoder into a set of latents: $\mathbf{z}_{bg} = \text{E}(\mathbf{v}_{bg})$. The background features are then integrated with the main video latents through concatenation: $\mathbf{z}_{final} = \text{CONCAT}([\mathbf{z}, \mathbf{z}_{bg}])$. For scenarios without background composition, we utilize a zero latent: $\mathbf{z}_{final} = \text{CONCAT}([\mathbf{z}, \mathbf{0}])$.

Diffusion Formulation. Inspired by SD3 [Esser et al. 2024], our framework adopts flow matching for the diffusion process. Given a timestep t , we perturb the original video x_0 following: $x_t = (1 - t)x_0 + t\epsilon$, $\epsilon \sim \mathcal{N}(0, \mathbf{I})$. The network is trained to predict the flow field $\mathbf{v} = x_0 - \epsilon$, offering improved stability and training efficiency compared to conventional diffusion approaches.

Implementation Details. Additional details on network architecture design, hyperparameter selection, and training are included in the supplement. We will release code and pretrained model.

6 EXPERIMENTS

6.1 Data

For *VAE training*, we utilize the Kinetics-600 [Kay et al. 2017] and Human4DiT [Shao et al. 2024] datasets. Additionally, we curate a custom evaluation dataset comprising 200 human videos featuring multi-person interactions, complex textures, and fast motion sequences.

For *DiT training*, we curate a dataset comprising 1M real human videos and 100K synthetic videos rendered using the PointOdyssey pipeline [Zheng et al. 2023a]. The real human videos are sourced from existing datasets including Human4DiT [Shao et al. 2024], Pexel, OpenVID-1M [Nan et al. 2024], MiraData [Ju et al. 2024], and Koala-36M [Wang et al. 2024]. The synthetic data is generated using 200 digital human models animated with motion sequences sampled from the CMU [Carnegie Mellon University 2014] and

Table 2. **Quantitative comparison of generated videos.** We compare our method with state-of-the-art baselines AnimateAnyone [Hu et al. 2023b], Champ [Zhu et al. 2024], MusePose [Tong et al. 2024], Animate-X [Tan et al. 2024], and Human4DiT [Shao et al. 2024] using multiple metrics (PSNR, SSIM, LPIPS, and FVD). Specifically, we evaluate three scenarios: videos with a static background (“Video”), with camera movement (“Camera”), and with background mask applied (“Mask”). Our approach achieves superior quality across all metrics and all scenarios.

Method	PSNR \uparrow			SSIM \uparrow			LPIPS \downarrow			FVD \downarrow		
	Video	Camera	Mask	Video	Camera	Mask	Video	Camera	Mask	Video	Camera	Mask
AnimateAnyone	19.39	18.87	26.99	0.757	0.656	0.953	0.211	0.234	0.058	693.9	935.9	234.7
Champ	21.72	20.04	26.34	0.819	0.712	0.954	0.126	0.204	0.041	466.8	872.3	181.7
MusePose	22.19	20.75	23.80	0.830	0.708	0.940	0.119	0.195	0.048	481.0	1135	264.4
Animate-X	23.03	21.67	29.84	0.839	0.719	0.965	0.116	0.163	0.039	285.3	608.4	147.7
Human4DiT	24.71	22.24	27.68	0.889	0.767	0.957	0.109	0.213	0.031	388.2	623.9	162.3
ISA-DiT (ours)	28.34	27.78	32.06	0.931	0.855	0.976	0.049	0.071	0.014	143.6	227.9	81.3

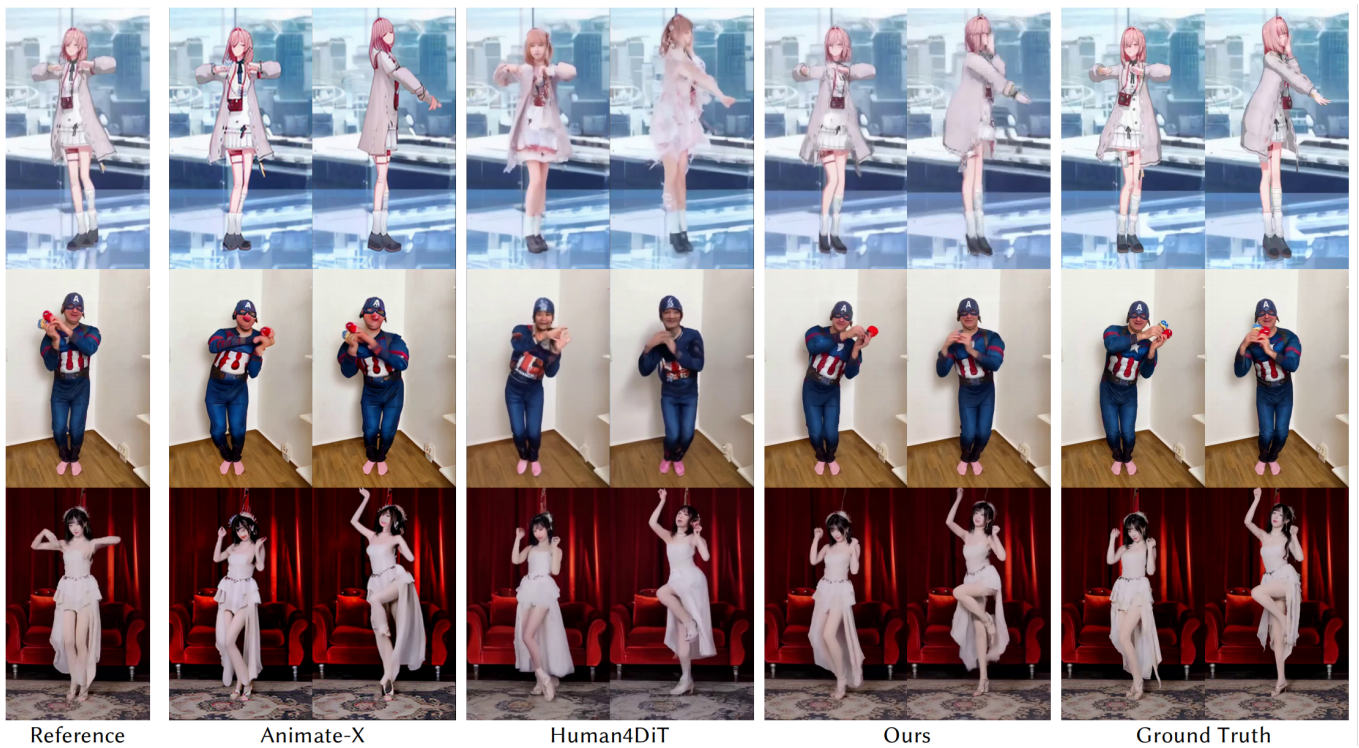


Fig. 9. **Qualitative comparisons of generated videos.** We compare our approach with the best-performing baselines; each of these methods is conditioned on the reference image shown on the left. Our method achieves superior visual quality, particularly in capturing facial expressions, modeling clothing dynamics, and rendering natural hand-object interactions.

AMASS [Mahmood et al. 2019] datasets. These animations are rendered in 1,000 different environment maps using procedurally generated camera trajectories, producing 100K videos at resolutions ranging from 512×512 to 1024×1024 . Since the synthetic data are highly controlled as we can directly export ground truth SMPL poses, camera poses, and backgrounds from the rendering engine. For the real human videos, we obtain SMPL annotations using Humans-in-4D [Goel et al. 2023] and segment the background on 1M videos

using SAM2 [Ravi et al. 2024]. For camera condition learning, we only utilize the camera poses from the synthetic data.

For *DiT evaluation*, we construct several test sets to evaluate different aspects of the model:

- “Video” Dataset: We collect 100 monocular human videos with static cameras, focusing on pure human motion without camera movement. This dataset serves to evaluate our method’s performance in human animation generation.

- “Camera” Dataset: This subset consists of 100 videos featuring both human motion and camera movement. It is designed to assess our method’s ability to generate 4D human scene videos with dynamic camera trajectories.
- “Mask” Dataset: We create a dedicated dataset of 100 videos with camera motion where backgrounds are masked out. This dataset evaluates the generated performance for the digital human(s) without considering the complex backgrounds.

These carefully curated datasets enable comprehensive evaluation of our model across three key aspects: human motion synthesis under static views, 4D human–scene generation with moving cameras, and isolated human motion generation with masked backgrounds.

6.2 Settings

Baselines. We compare our method with several state-of-the-art approaches for human video generation, including AnimateAnyone [Hu et al. 2023b], CHAMP [Zhu et al. 2024], MusePose [Tong et al. 2024], Animate-X [Tan et al. 2024], and Human4DiT [Shao et al. 2024]. Since the official implementation of AnimateAnyone is not publicly available, we utilize the PyTorch version implemented by Moore-AnimateAnyone for our experiments. For AnimateAnyone, MusePose, and Animate-X, we employ DWPose [Yang et al. 2023] to extract human pose estimations from the input videos, generating skeleton graphs as conditional inputs. For CHAMP, following the official pipeline, we simultaneously estimate SMPL parameters and render the corresponding depth maps, normal maps, and semantic segmentation masks of the motion videos, along with DWPose skeleton graphs as conditional inputs. For Human4DiT, we estimate SMPL parameters to render SMPL normal maps and use DPVO [Teed et al. 2023] to estimate camera parameters from the motion videos as conditional inputs. Given that all these methods employ image-based VAE architectures with limited temporal inference windows, we adopt a sliding window approach during inference with a window size of 24 frames and an overlap of 8 frames between consecutive windows. For fair comparison, all methods use 30 sampling steps with the DDIM [Song et al. 2020] scheduler during inference.

SOTA image-to-video models. To evaluate the generative ability of our model for human-centric videos, we conduct comprehensive comparisons with SOTA image-to-video models, including Cosmos [Agarwal et al. 2025], Hunyuan [Kong et al. 2024] and Wan [Wang et al. 2025] using the VBench [Huang et al. 2024a] benchmark suite.

Evaluation Metrics. To evaluate our pose-driven image-to-video generation model, we employ both frame-level and video-level metrics. For individual frames, we assess generation quality using standard metrics: PSNR, SSIM, and LPIPS [Zhang et al. 2018]. For video-level evaluation, we measure generation quality using Fréchet Video Distance (FVD) [Unterthiner et al. 2019].

CFG Scales. We observe that classifier-free guidance (CFG) plays a crucial role in video generation quality. At CFG=1, generated videos exhibit noticeable blurriness, motion blur, and lack fine details. Conversely, high CFG values produce overly sharp videos

Table 3. **Quantitative comparison based on VBench.** We compare our method with state-of-the-art image-to-video methods including Cosmos [Reda et al. 2024], Hunyuan [Kong et al. 2024], and WAN2.1 [Wang et al. 2025] using multiple metrics (Quality, Aesthetics, and Consistency).

Method	Quality↑	Aesthetics↑	Consistency↑
Cosmos-I2V-14B	0.693	0.528	0.896
Hunyuan-I2V-14B	0.705	0.546	0.904
WAN2.1-I2V-14B	0.738	0.582	0.929
ISA-DiT(ours)-4B	0.724	0.579	0.953

with texture artifacts. In our experiments, we employ CFG=2 while comparison methods are evaluated using their default CFG settings.

6.3 Evaluation

Quantitative Comparisons. We perform comprehensive quantitative comparisons on the DiT evaluation datasets in Tab. 2. Our ISA-DiT shows improvements over the baselines across key metrics, including PSNR, SSIM, LPIPS, and FVD. These quantitative results suggest that our model is better at generating detailed and consistent human videos. Our method performs particularly well in scenarios involving camera motion, demonstrating effective handling of both human animation and scene dynamics.

Additionally, we utilize VBench to evaluate and compare the generation capability of our model with current open-source image-to-video generation models, where we select the first frame of the videos in our proposed “Video Dataset” as the input image. As shown in Tab. 3, our model achieves performance comparable to current open-source large video models, with significantly smaller model sizes and greater efficiency, demonstrating the effectiveness of our proposed ISA and model design.

Qualitative Comparisons. We compare our method qualitatively against state-of-the-art approaches, with results shown in Fig. 9 and the supplemental video. Here, we focus on the best-performing baselines—Human4DiT and Animate-X; additional results are provided in the supplement. Our method demonstrates superior quality in human video generation, which is most noticeable in facial details, body structure, and dynamic motion. Our generated videos also show improved quality in natural movements, including realistic hair dynamics, clothing deformation, and hand–object interactions. These results validate our method’s ability to effectively learn to generate complex dynamic features, leading to more coherent and realistic human videos.

Camera Control. We present generated human videos with diverse camera trajectories in Fig. 10 and the supplemental video, illustrating our method’s ability to jointly control human motion and background changes under camera movement. Leveraging our interspatial attention block, our model produces view-consistent human–scene videos with a high level of multi-view consistency and dynamic camera control.

Multi-character Animation. Our method supports multiple digital humans in the same video, as shown in Fig. 11. This capability stems from our identity control module and ISA mechanism, which

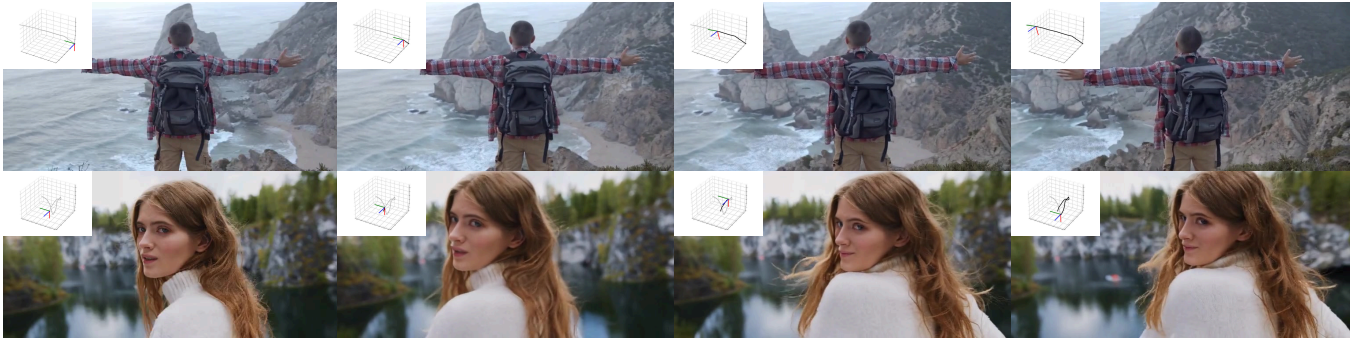


Fig. 10. **Generating videos with controllable camera trajectories.** Our model can generate high-quality human videos conditioned on specific camera trajectories (top left insets), effectively transforming video generation into a dynamic view-synthesis system for multi-view human generation.



Fig. 11. **Generating multiple characters.** Our method synthesizes multi-character videos featuring realistic interactions, such as dancing and boxing.

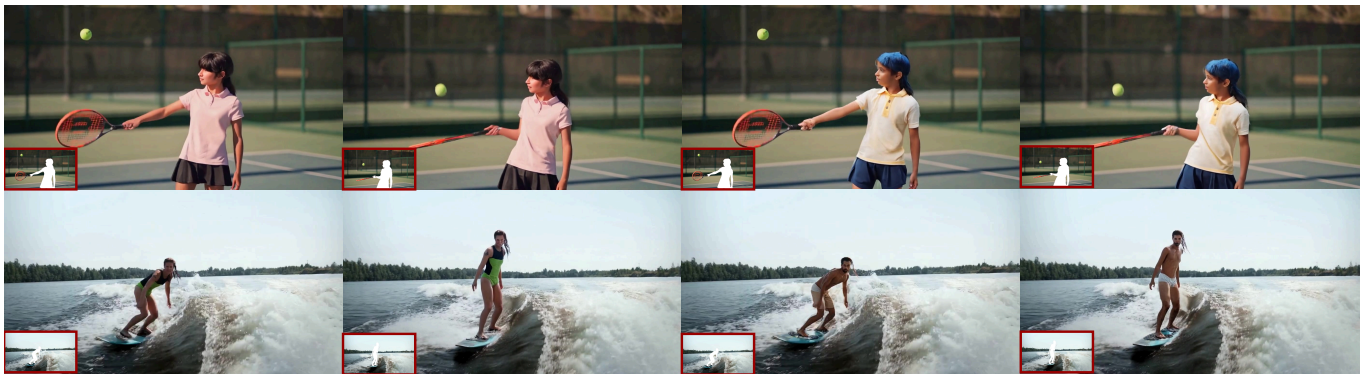


Fig. 12. **Human video generation with controlled backgrounds.** Our method generates videos by compositing synthesized digital humans with background scenes, achieving consistent lighting and shadow effects based on background conditions.

flexibly maps between generated video content and SMPL conditions regardless of the number of input characters. Specifically, we first track and obtain the SMPL for each individual, then sample points from each person’s SMPL to generate tokens which are concatenated and fed into the ISA block. Through this injection, we effectively maintain identity consistency and achieve superior spatiotemporal coherence.

Background Composition. Our method also enables creative applications in human–background video compositing. As demonstrated in Fig. 12, our method is able to generate different characters using the same background video, with composite videos maintain consistency in lighting, shadows, and perspective between the generated human and the background environment. Similarly, we could generate the same character in front of different backgrounds (not shown).



Fig. 13. **Additional generated videos.** Our ISA-DiT framework generates high-quality videos across diverse domains, spanning upper-body portraits, full-body movements, anime character and multi-characters animations.

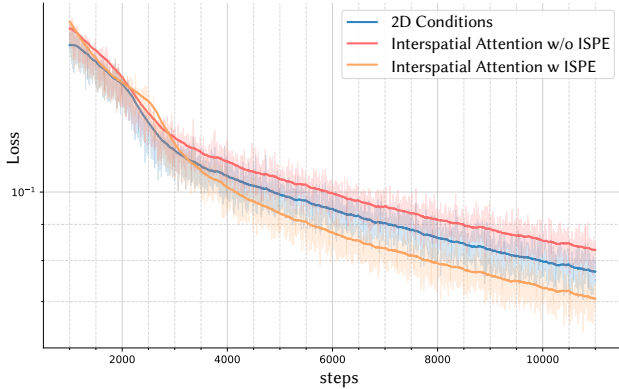


Fig. 14. **Ablation of interspatial attention.** We compare validation loss curves for the same DiT architecture using three different conditioning mechanisms: a baseline that only uses the 2D SMPL normal maps for conditioning, ISA without interspatial positional encoding, and interspatial attention with positional encoding. The latter conditioning converges faster and to a lower loss value than the other options.

Table 4. **Ablation Study.** We conduct an ablation study on our proposed ISA and different 3D template control signals. “Ours (W/o ISPE)” refers to using ISA without the proposed ISPE, while “Ours (2D ControlNet)” refers to not using ISA and instead employing 2D ControlNet for SMPL-based conditioning. Across different 3D templates, we compared the facial generation capabilities of both SMPL and FLAME models.

Method	PSNR \uparrow	SSIM \uparrow	LPIPS \downarrow	FVD \downarrow
Ours (W/o ISPE)	25.21	0.895	0.079	230.2
Ours (2D ControlNet)	26.45	0.916	0.064	195.7
Ours	28.34	0.931	0.049	143.6
Face (SMPL)	30.42	0.955	0.039	112.4
Face (FLAME)	31.05	0.972	0.034	101.9

Additional Results. To comprehensively showcase the capabilities of our method, we present an extensive collection of generation results in Fig. 13 and the supplementary video. Our method handles a diverse range of scenarios, including facial animations, upper-body portrait videos, full-body animations, multi-person interactions, and anime character generation. The consistent performance across varied applications indicates the method’s adaptability and generalization capabilities.

6.4 Ablation Study

ISA mechanism. To validate the effectiveness of our ISA mechanism, we run an ablation to compare three variants of our DiT: (1) a baseline without ISA, where SMPL conditions are rendered directly into 2D normal maps, which are used as conditioning input; (2) ISA without position encoding; and (3) ISA with position encoding. Fig. 14 shows the validation loss curves for each configuration. During early training, all variants converge quickly. As training progresses, the position-encoded ISA variant establishes stronger 3D–2D correlations leading to faster convergence and lower a validation loss compared to the other configurations. Additionally, Fig. 15 and

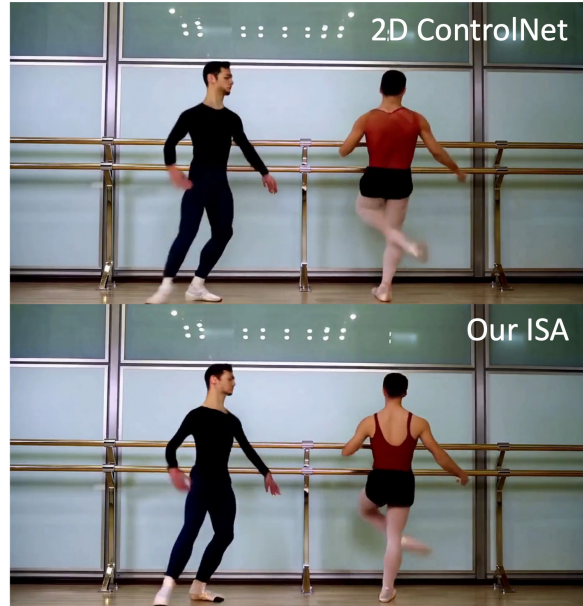


Fig. 15. **Ablation of interspatial attention.** We show qualitative comparisons between 2D ControlNet and ISA. For complex 3D poses, the ControlNet produces implausible deformations while our ISA generates more natural and realistic human motions.



Fig. 16. **ISA with 3D FLAME for expression generation.** ISA could be effectively integrated with more precise 3D face models like FLAME to achieve vivid facial generation.

Tab. 4 demonstrate qualitative and quantitative results. For videos involving fast movements and complex 3D poses, the ControlNet variant produces implausible deformations while our ISA generates more natural and realistic human motions. This experiment clearly validates the effectiveness of our ISA design.

3D Template Model. Additionally, we explore the use of an alternative 3D face model, i.e., FLAME [Li et al. 2017], to enhance ISA’s facial modeling. We evaluate it on 100 face-centric videos using the FLAME model as conditions. Tab. 4 shows improvements across all metrics from SMPL to FLAME. With 3D FLAME, ISA can generate

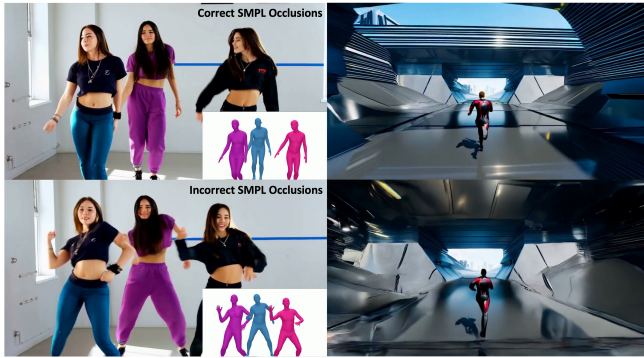


Fig. 17. **Failure cases.** Our method generates photorealistic multi-character videos given accurate SMPL estimations (top left), but fails when inter-character occlusions are incorrectly estimated (bottom left). Rapid camera movements also introduce background distortions, as shown on the right (top: reference image; bottom: results with aggressive viewpoint changes).

vivid human expressions as shown in Fig. 16. This demonstrates ISA could be effectively integrated with more precise 3D face models to achieve superior facial generation.

6.5 Scaling.

We perform additional experiments that validate the effectiveness of ISA when scaling the DiT architecture in the supplement.

7 DISCUSSION

Limitations. While our approach successfully generates natural and realistic videos from imprecise SMPL estimates, it still relies on these SMPL estimations as input. In complex scenarios with multiple interacting people, errors in estimating occlusion relationships between SMPL models can lead to significant artifacts in the generated videos, as shown in Fig. 17. Additionally, although our model can generate camera-controllable human videos, it struggles with cases involving extreme camera variations. This limitation is particularly evident in background generation across wide viewpoint ranges as shown in Fig. 17. The challenge of generating consistent and realistic backgrounds across 360 degrees is substantial, requiring significantly larger models and extensive video training datasets to achieve satisfactory results.

Ethics Considerations. Our research presents advanced generative AI capabilities for human video synthesis. We firmly oppose the misuse of our technology for generating manipulated content of real individuals. While our model enables the creation and editing of photorealistic digital humans, we strongly condemn any application aimed at spreading misinformation, damaging reputations, or creating deceptive content. We acknowledge the ethical considerations surrounding this technology and are committed to responsible development and deployment that prioritizes transparency and prevents harmful applications.

Conclusion. In summary, we introduce a novel and scalable interspatial attention (ISA) mechanism that seamlessly integrates

with modern, scalable diffusion transformers to address the challenges of controllable photorealistic 4D human video generation. Through the combination of ISA, which leverages specialized 3D–2D relative positional encodings, and a custom video VAE, our approach achieves a significantly higher quality and consistency than baselines. Our model’s ability to maintain precise control over camera and human poses while generating high-quality videos of multiple humans represents a significant advancement in the field of human video generation.

Acknowledgment. We would like to thank Shengqu Cai, He Hao, and Kecheng Zheng for their valuable discussions and insightful suggestions throughout the development of this work. We also thank all co-authors for their contributions and collaboration on this project.

REFERENCES

- Rameen Abdal, Wang Yifan, Zifan Shi, Yinghao Xu, Ryan Po, Zhengfei Kuang, Qifeng Chen, Dit-Yan Yeung, and Gordon Wetzstein. 2024. Gaussian shell maps for efficient 3d human generation. In *Proceedings of the IEEE/CVF Conference on Computer Vision and Pattern Recognition*. 9441–9451.
- Niket Agarwal, Arslan Ali, Maciej Bala, Yogesh Balaji, Erik Barker, Tiffany Cai, Prithvijit Chattopadhyay, Yongxin Chen, Yin Cui, Yifan Ding, et al. 2025. Cosmos world foundation model platform for physical ai. *arXiv preprint arXiv:2501.03575* (2025).
- Alexander Bergman, Petr Kellnhofer, Wang Yifan, Eric Chan, David Lindell, and Gordon Wetzstein. 2022. Generative neural articulated radiance fields. *Advances in Neural Information Processing Systems* 35 (2022), 19900–19916.
- Ankan Kumar Bhunia, Salman Khan, Hisham Cholakkal, Rao Muhammad Anwer, Jorma Laaksonen, Mubarak Shah, and Fahad Shahbaz Khan. 2023. Person image synthesis via denoising diffusion model. In *Proceedings of the IEEE/CVF Conference on Computer Vision and Pattern Recognition*. 5968–5976.
- Carnegie Mellon University. 2014. CMU MoCap Dataset. <http://mocap.cs.cmu.edu>
- Patrick Esser, Sumith Kulal, Andreas Blattmann, Rahim Entezari, Jonas Müller, Harry Saini, Yam Levi, Dominik Lorenz, Axel Sauer, Frederic Boesel, Dustin Podell, Tim Dockhorn, Zion English, and Robin Rombach. 2024. Scaling Rectified Flow Transformers for High-Resolution Image Synthesis. In *Forty-first International Conference on Machine Learning, ICML 2024, Vienna, Austria, July 21–27, 2024*. OpenReview.net.
- Patrick Esser, Robin Rombach, and Bjorn Ommer. 2021. Taming transformers for high-resolution image synthesis. In *Proceedings of the IEEE/CVF conference on computer vision and pattern recognition*. 12873–12883.
- Songwei Ge, Thomas Hayes, Harry Yang, Xi Yin, Guan Pang, David Jacobs, Jia-Bin Huang, and Devi Parikh. 2022. Long video generation with time-agnostic vqgan and time-sensitive transformer. In *European Conference on Computer Vision*, Springer, 102–118.
- Shubham Goel, Georgios Pavlakos, Jathushan Rajasegaran, Angjoo Kanazawa*, and Jitendra Malik*. 2023. Humans in 4D: Reconstructing and Tracking Humans with Transformers. In *International Conference on Computer Vision (ICCV)*.
- Ian Goodfellow, Jean Pouget-Abadie, Mehdi Mirza, Bing Xu, David Warde-Farley, Sherjil Ozair, Aaron Courville, and Yoshua Bengio. 2014. Generative adversarial nets. *Advances in neural information processing systems* 27 (2014).
- Agrim Gupta, Lijun Yu, Kihyuk Sohn, Xiuye Gu, Meera Hahn, Li Fei-Fei, Irfan Essa, Lu Jiang, and José Lezama. 2023. Photorealistic video generation with diffusion models. *arXiv preprint arXiv:2312.06662* (2023).
- Hao He, Yinghao Xu, Yuwei Guo, Gordon Wetzstein, Bo Dai, Hongsheng Li, and Ceyuan Yang. 2024. CameraCtrl: Enabling Camera Control for Text-to-Video Generation. *arXiv:2404.02101 [cs.CV]*
- Li Hu, Xin Gao, Peng Zhang, Ke Sun, Bang Zhang, and Liefeng Bo. 2023a. Animate anyone: Consistent and controllable image-to-video synthesis for character animation. *arXiv preprint arXiv:2311.17117* (2023).
- Li Hu, Xin Gao, Peng Zhang, Ke Sun, Bang Zhang, and Liefeng Bo. 2023b. Animate Anyone: Consistent and Controllable Image-to-Video Synthesis for Character Animation. *arXiv preprint arXiv:2311.17117* (2023).
- Xin Huang, Ruizhi Shao, Qi Zhang, Hongwen Zhang, Ying Feng, Yebin Liu, and Qing Wang. 2024b. Humannorm: Learning normal diffusion model for high-quality and realistic 3d human generation.
- Ziqi Huang, Yinan He, Jiashuo Yu, Fan Zhang, Chenyang Si, Yuming Jiang, Yuanhan Zhang, Tianxing Wu, Qingyang Jin, Nattapol Chanpaisit, Yaohui Wang, Xinyuan Chen, Limin Wang, Dahua Lin, Yu Qiao, and Ziwei Liu. 2024a. VBench: Comprehensive Benchmark Suite for Video Generative Models. In *Proceedings of the IEEE/CVF Conference on Computer Vision and Pattern Recognition*.

- Xuan Ju, Yiming Gao, Zhaoyang Zhang, Ziyang Yuan, Xintao Wang, Ailing Zeng, Yu Xiong, Qiang Xu, and Ying Shan. 2024. *Miradata: A large-scale video dataset with long durations and structured captions*. *Advances in Neural Information Processing Systems* 37 (2024), 48955–48970.
- Johanna Karras, Aleksander Holynski, Ting-Chun Wang, and Ira Kemelmacher-Shlizerman. 2023. *Dreampose: Fashion video synthesis with stable diffusion*. In *Proceedings of the IEEE/CVF International Conference on Computer Vision*. 22680–22690.
- Will Kay, Joao Carreira, Karen Simonyan, Brian Zhang, Chloe Hillier, Sudheendra Vijayanarasimhan, Fabio Viola, Tim Green, Trevor Back, Paul Natsev, et al. 2017. *The kinetics human action video dataset*. *arXiv preprint arXiv:1705.06950* (2017).
- Diederik P Kingma. 2013. *Auto-encoding variational bayes*. *arXiv preprint arXiv:1312.6114* (2013).
- Nikos Kolotouros, Thimo Alldieck, Andrei Zanfir, Eduard Gabriel Bazavan, Mihai Fieraru, and Cristian Sminchisescu. 2023. *DreamHuman: Animatable 3D Avatars from Text*. (2023).
- Weijie Kong, Qi Tian, Zijian Zhang, Rox Min, Zuozhuo Dai, Jin Zhou, Jiangfeng Xiong, Xin Li, Bo Wu, Jianwei Zhang, Kathrina Wu, Qin Lin, Aladdin Wang, Andong Wang, Changlin Li, DuoJun Huang, Fang Yang, Hao Tan, Hongmei Wang, Jacob Song, Jiawang Bai, Jianbing Wu, Jinbao Xue, Joey Wang, Junkun Yuan, Kai Wang, Mengyang Liu, Pengyu Li, Shuai Li, Weiyang Wang, Wenqing Yu, Xincheng Deng, Yang Li, Yanxin Long, Yi Chen, Yutao Cui, Yuanbo Peng, Zhentao Yu, Zhiyu He, Zhiyong Xu, Zixiang Zhou, Zunnan Xu, Yangyu Tao, Qinglin Lu, Songtao Liu, Daquan Zhou, Hongfa Wang, Yong Yang, Di Wang, Yuhong Liu, Jie Jiang, and Caesar Zhong. 2024. *HunyuanVideo: A Systematic Framework For Large Video Generative Models*. *arXiv preprint arXiv:2412.03603* (2024). <https://arxiv.org/abs/2412.03603>
- Jimmy Lei Ba, Jamie Ryan Kiros, and Geoffrey E Hinton. 2016. *Layer normalization*. *ArXiv e-prints* (2016), arXiv-1607.
- Tianye Li, Timo Bolkart, Michael J. Black, Hao Li, and Javier Romero. 2017. *Learning a model of facial shape and expression from 4D scans*. *ACM Transactions on Graphics, (Proc. SIGGRAPH Asia)* 36, 6 (2017), 194:1–194:17. <https://doi.org/10.1145/3130800.3130813>
- Zhe Li, Zerong Zheng, Lizhen Wang, and Yebin Liu. 2024. *Animatable gaussians: Learning pose-dependent gaussian maps for high-fidelity human avatar modeling*. In *Proceedings of the IEEE/CVF Conference on Computer Vision and Pattern Recognition*. 19711–19722.
- Tingting Liao, Hongwei Yi, Yuliang Xu, Jiayang Tang, Yangyi Huang, Justus Thies, and Michael J Black. 2023. *TADA! Text to Animatable Digital Avatars*. *ArXiv* (Aug 2023).
- Lingjie Liu, Marc Habermann, Viktor Rudnev, Kripasindhu Sarkar, Jiatao Gu, and Christian Theobalt. 2021. *Neural actor: Neural free-view synthesis of human actors with pose control*. *ACM transactions on graphics (TOG)* 40, 6 (2021), 1–16.
- Xian Liu, Xiaohang Zhan, Jiayang Tang, Ying Shan, Gang Zeng, Dahua Lin, Xihui Liu, and Ziwei Liu. 2023. *HumanGaussian: Text-Driven 3D Human Generation with Gaussian Splatting*. *arXiv preprint arXiv:2311.17061* (2023).
- Matthew Loper, Naureen Mahmood, Javier Romero, Gerard Pons-Moll, and Michael J Black. 2023. *SMPL: A skinned multi-person linear model*. In *Seminal Graphics Papers: Pushing the Boundaries, Volume 2*. 851–866.
- LumaAI. 2024. *Luma Dream Machine*. <https://lumalabs.ai/dream-machine>. Accessed: 2025-01-22.
- Zhuoyan Luo, Fengyuan Shi, Yixiao Ge, Yujiu Yang, Limin Wang, and Ying Shan. 2024. *Open-magvit2: An open-source project toward democratizing auto-regressive visual generation*. *arXiv preprint arXiv:2409.04410* (2024).
- Naureen Mahmood, Nima Ghorbani, Nikolaus F. Troje, Gerard Pons-Moll, and Michael J. Black. 2019. *AMASS: Archive of Motion Capture as Surface Shapes*. In *Proceedings of the IEEE/CVF International Conference on Computer Vision (ICCV)*. 5441–5450.
- Lars Mescheder, Michael Oechsle, Michael Niemeyer, Sebastian Nowozin, and Andreas Geiger. 2019. *Occupancy Networks: Learning 3D Reconstruction in Function Space*. In *CVPR*.
- Ben Mildenhall, Pratul P Srinivasan, Matthew Tancik, Jonathan T Barron, Ravi Ramamoorthi, and Ren Ng. 2020. *Nerf: Representing scenes as neural radiance fields for view synthesis*. In *ECCV*.
- Mehdi Mirza and Simon Osindero. 2014. *Conditional generative adversarial nets*. *arXiv preprint arXiv:1411.1784* (2014).
- Mochi-Team. 2024. *Mochi*. <https://github.com/Mochi-Team/mochi>.
- Kepan Nan, Rui Xie, Penghao Zhou, Tiehan Fan, Zhenheng Yang, Zhijie Chen, Xiang Li, Jian Yang, and Ying Tai. 2024. *Openvid-1m: A large-scale high-quality dataset for text-to-video generation*. *arXiv preprint arXiv:2407.02371* (2024).
- OpenAI. 2024. *Video generation models as world simulators*. <https://openai.com/index/video-generation-models-as-world-simulators/>. Accessed: 2024-05-19.
- Jeong Joon Park, Peter Florence, Julian Straub, Richard Newcombe, and Steven Lovegrove. 2019. *DeepSDF: Learning continuous signed distance functions for shape representation*. In *CVPR*.
- Nikhila Ravi, Valentin Gabeur, Yuan-Ting Hu, Ronghang Hu, Chaitanya Ryali, Tengyu Ma, Haitham Khedr, Roman Rädle, Chloe Rolland, Laura Gustafson, et al. 2024. *Sam 2: Segment anything in images and videos*. *arXiv preprint arXiv:2408.00714* (2024).
- Fitsum Reda, Jinwei Gu, Xian Liu, Songwei Ge, Ting-Chun Wang, Haoxiang Wang, and Ming-Yu Liu. 2024. *Cosmos-Tokenizer*. <https://github.com/NVIDIA/Cosmos-Tokenizer>.
- Robin Rombach, Andreas Blattmann, Dominik Lorenz, Patrick Esser, and Björn Ommer. 2022. *High-resolution image synthesis with latent diffusion models*. In *Proceedings of the IEEE/CVF conference on computer vision and pattern recognition*. 10684–10695.
- RunwayAI. 2025. *Runway Gen-3*. <https://runwayml.com/>. Accessed: 2025-01-22.
- Ruizhi Shao, Youxin Pang, Zerong Zheng, Jingxiang Sun, and Yebin Liu. 2024. *Human4DiT: Free-view Human Video Generation with 4D Diffusion Transformer*. *arXiv preprint arXiv:2405.17405* (2024).
- Aliaksandr Siarohin, Stéphane Lathuilière, Enver Sangineto, and Nicu Sebe. 2019a. *Appearance and pose-conditioned human image generation using deformable gans*. *IEEE transactions on pattern analysis and machine intelligence* 43, 4 (2019), 1156–1171.
- Aliaksandr Siarohin, Stéphane Lathuilière, Sergey Tulyakov, Elisa Ricci, and Nicu Sebe. 2019b. *First order motion model for image animation*. *Advances in neural information processing systems* 32 (2019).
- Aliaksandr Siarohin, Enver Sangineto, Stéphane Lathuilière, and Nicu Sebe. 2018. *Deformable gans for pose-based human image generation*. In *Proceedings of the IEEE conference on computer vision and pattern recognition*. 3408–3416.
- Jiaming Song, Chenlin Meng, and Stefano Ermon. 2020. *Denoising Diffusion Implicit Models*. *arXiv:2010.02502* (October 2020). <https://arxiv.org/abs/2010.02502>
- Shuai Tan, Biao Gong, Xiang Wang, Shiwei Zhang, Dandan Zheng, Ruobing Zheng, Kecheng Zheng, Jingdong Chen, and Ming Yang. 2024. *Animate-x: Universal character image animation with enhanced motion representation*. *arXiv preprint arXiv:2410.10306* (2024).
- Zachary Teed, Lahav Lipson, and Jia Deng. 2023. *Deep Patch Visual Odometry*. *Advances in Neural Information Processing Systems* (2023).
- Yu Tian, Jian Ren, Menglei Chai, Kyle Olszewski, Xi Peng, Dimitris N Metaxas, and Sergey Tulyakov. 2021. *A good image generator is what you need for high-resolution video synthesis*. *arXiv preprint arXiv:2104.15069* (2021).
- Zhengyan Tong, Chao Li, Zhaokang Chen, Bin Wu, and Wenjiang Zhou. 2024. *MusePose: A Pose-Driven Image-to-Video Framework for Virtual Human Generation*. *arXiv* (2024).
- Thomas Unterthiner, Sjoerd van Steenkiste, Karol Kurach, Raphaël Marinier, Marcin Michalewski, and Sylvain Gelly. 2019. *FVD: A new metric for video generation*. (2019).
- Dani Valevski, Yaniv Leviathan, Moab Arar, and Shlomi Fruchter. 2024. *Diffusion Models Are Real-Time Game Engines*. *arXiv:2408.14837 [cs.LG]* <https://arxiv.org/abs/2408.14837>
- Aaron Van Den Oord, Oriol Vinyals, et al. 2017. *Neural discrete representation learning*. *Advances in neural information processing systems* 30 (2017).
- Ashish Vaswani, Noam Shazeer, Niki Parmar, Jakob Uszkoreit, Llion Jones, Aidan N Gomez, Łukasz Kaiser, and Illia Polosukhin. 2017. *Attention is all you need*. *Advances in neural information processing systems* 30 (2017).
- Ruben Villegas, Mohammad Babaeizadeh, Pieter-Jan Kindermans, Hernan Moraldo, Han Zhang, Mohammad Taghi Saffar, Santiago Castro, Julius Kunze, and Dumitru Erhan. 2022. *Phenaki: Variable length video generation from open domain textual descriptions*. In *International Conference on Learning Representations*.
- Ang Wang, Baole Ai, Bin Wen, Chaojie Mao, Chen-Wei Xie, Di Chen, Feiwu Yu, Haiming Zhao, Jianxiao Yang, Jianyuan Zeng, et al. 2025. *Wan: Open and Advanced Large-Scale Video Generative Models*. *arXiv preprint arXiv:2503.20314* (2025).
- Qiheng Wang, Yukai Shi, Jiarong Ou, Rui Chen, Ke Lin, Jiahao Wang, Boyuan Jiang, Haotian Yang, Mingwu Zheng, Xin Tao, et al. 2024. *Koala-36m: A large-scale video dataset improving consistency between fine-grained conditions and video content*. *arXiv preprint arXiv:2410.08260* (2024).
- Tan Wang, Linjie Li, Kevin Lin, Chung-Ching Lin, Zhengyuan Yang, Hanwang Zhang, Zicheng Liu, and Lijuan Wang. 2023. *Disco: Disentangled control for referring human dance generation in real world*. *arXiv e-prints* (2023), arXiv-2307.
- Ting-Chun Wang, Arun Mallya, and Ming-Yu Liu. 2021. *One-shot free-view neural talking-head synthesis for video conferencing*. In *Proceedings of the IEEE/CVF conference on computer vision and pattern recognition*. 10039–10049.
- Yaohui Wang, Piotr Bilinski, Francois Bremond, and Antitza Dantcheva. 2020. *G3AN: Disentangling appearance and motion for video generation*. In *Proceedings of the IEEE/CVF Conference on Computer Vision and Pattern Recognition*. 5264–5273.
- Chung-Yi Weng, Brian Curless, Pratul P Srinivasan, Jonathan T Barron, and Ira Kemelmacher-Shlizerman. 2022. *Humannerf: Free-viewpoint rendering of moving people from monocular video*. In *Proceedings of the IEEE/CVF conference on computer vision and pattern recognition*. 16210–16220.
- Zhongcong Xu, Jianfeng Zhang, Jun Hao Liew, Hanshu Yan, Jia-Wei Liu, Chenxu Zhang, Jiashi Feng, and Mike Zheng Shou. 2024. *MagicAnimate: Temporally Consistent Human Image Animation using Diffusion Model*.
- Wilson Yan, Yunzhi Zhang, Pieter Abbeel, and Aravind Srinivas. 2021. *Videopt: Video generation using vq-vae and transformers*. *arXiv preprint arXiv:2104.10157* (2021).
- Shiyuan Yang, Liang Hou, Haibin Huang, Chongyang Ma, Pengfei Wan, Di Zhang, Xiaodong Chen, and Jing Liao. 2024a. *Direct-a-Video: Customized Video Generation*

- with User-Directed Camera Movement and Object Motion. [arXiv preprint arXiv:2402.03162 \(2024\)](#).
- Zhuoyi Yang, Jiayan Teng, Wendi Zheng, Ming Ding, Shiyu Huang, Jiazheng Xu, Yuanming Yang, Wenyi Hong, Xiaohan Zhang, Guanyu Feng, et al. 2024b. Cogvideox: Text-to-video diffusion models with an expert transformer. [arXiv preprint arXiv:2408.06072 \(2024\)](#).
- Zhendong Yang, Ailing Zeng, Chun Yuan, and Yu Li. 2023. Effective whole-body pose estimation with two-stages distillation. In *Proceedings of the IEEE/CVF International Conference on Computer Vision*. 4210–4220.
- Jiahui Yu, Xin Li, Jing Yu Koh, Han Zhang, Ruoming Pang, James Qin, Alexander Ku, Yuanzhong Xu, Jason Baldridge, and Yonghui Wu. 2021. Vector-quantized image modeling with improved vqgan. [arXiv preprint arXiv:2110.04627 \(2021\)](#).
- Lijun Yu, Yong Cheng, Kihyuk Sohn, José Lezama, Han Zhang, Huiwen Chang, Alexander G Hauptmann, Ming-Hsuan Yang, Yuan Hao, Irfan Essa, et al. 2023a. Magvit: Masked generative video transformer. In *Proceedings of the IEEE/CVF Conference on Computer Vision and Pattern Recognition*. 10459–10469.
- Lijun Yu, José Lezama, Nitesh B Gundavarapu, Luca Versari, Kihyuk Sohn, David Minnen, Yong Cheng, Vighnesh Birodkar, Agrim Gupta, Xiuye Gu, et al. 2023b. Language Model Beats Diffusion–Tokenizer is Key to Visual Generation. [arXiv preprint arXiv:2310.05737 \(2023\)](#).
- Richard Zhang, Phillip Isola, Alexei A Efros, Eli Shechtman, and Oliver Wang. 2018. The Unreasonable Effectiveness of Deep Features as a Perceptual Metric. In *CVPR*.
- Sijie Zhao, Yong Zhang, Xiaodong Cun, Shaoshu Yang, Muyao Niu, Xiaoyu Li, Wenbo Hu, and Ying Shan. 2024. CV-VAE: A Compatible Video VAE for Latent Generative Video Models. <https://arxiv.org/abs/2405.20279> (2024).
- Yang Zheng, Adam W Harley, Bokui Shen, Gordon Wetzstein, and Leonidas J Guibas. 2023a. Pointodyssey: A large-scale synthetic dataset for long-term point tracking. In *Proceedings of the IEEE/CVF International Conference on Computer Vision*. 19855–19865.
- Zangwei Zheng, Xiangyu Peng, Tianji Yang, Chenhui Shen, Shenggui Li, Hongxin Liu, Yukun Zhou, Tianyi Li, and Yang You. 2024. Open-Sora: Democratizing Efficient Video Production for All. <https://github.com/hpcaitech/Open-Sora>
- Zerong Zheng, Xiaochen Zhao, Hongwen Zhang, Boning Liu, and Yebin Liu. 2023b. Avatarrex: Real-time expressive full-body avatars. *ACM Transactions on Graphics (TOG)* 42, 4 (2023), 1–19.
- Shenhao Zhu, Junming Leo Chen, Zuozhuo Dai, Yinghui Xu, Xun Cao, Yao Yao, Hao Zhu, and Siyu Zhu. 2024. Champ: Controllable and Consistent Human Image Animation with 3D Parametric Guidance. In *European Conference on Computer Vision (ECCV)*.